LIDAR ACTIVITIES AT THE VIENNESE INSTITUTE OF PHOTOGRAMMETRY AND REMOTE SENSING

Franz Rottensteiner, Helmut Kager, Christian Briese, Karl Kraus

Institute of Photogrammetry and Remote Sensing, Vienna University of Technology
Gußhausstraße 27-29, A-1040 Vienna, Austria
{fr,hk,cb,kk}@ipf.tuwien.ac.at

ABSTRACT:

In the recent years, LIDAR has emerged as an efficient technology for capturing 3D data. In this paper, we will describe the activities of the Institute of Photogrammetry and Remote Sensing at Vienna University of Technology (I.P.F.) in the field of LIDAR processing. At the I.P.F., a method for filtering LIDAR data based on robust linear prediction has been developed. This filtering method has been applied for the automatic generation of digital terrain models. In densely built-up areas, the method has to be applied to thinned-out data first to eliminate large areas of points reflected at the roofs of buildings, which results in a hierarchic application of robust linear prediction. To improve the geomorphologic quality of digital terrain models derived from LIDAR data, break lines have to be detected in these data. Two techniques for that purpose developed at the I.P.F. are described in this paper. Hierarchic robust linear prediction can also be the basis for building extraction from LIDAR data: the points having been eliminated in DTM estimation are further classified according to whether they have been reflected on the tops of buildings or not, and connected regions of building points ("building regions") are further analysed with the goal of finding planar patches and grouping these patches to reconstruct polyhedral building models. Finally, the I.P.F.'s activities in the field of LIDAR calibration are described. This covers a method for simultaneous height fitting of LIDAR strips and a more sophisticated technique based on modelling both the flight paths and the sensor attitudes by splines.

1 INTRODUCTION

In the recent years, LIDAR has emerged as an efficient technology for capturing 3D data. It delivers 3D point clouds at a relatively high resolution of 1 point / m^2 and better, and the height accuracy it offers is well-suited for many applications in topographic mapping. In this context, LIDAR data have especially been used to generate digital terrain models (DTMs) and, higher and higher resolution becoming available, 3D city models in a relatively short turnout-time. LIDAR has turned out to be an efficient alternative to traditional photogrammetric techniques with a high potential for automation of the respective tasks for certain applications. The increasing importance of LIDAR in the photogrammetric community is well reflected in the number of LIDAR workshops and the number of papers dealing with LIDAR processing presented at the ISPRS mid-term symposium of Commission III (Kalliany and Leberl, 2002).

The problems that have to be tackled in mapping from LIDAR data are connected with three properties of LIDAR data:

1. It is the goal of topographic mapping to obtain a digital model of the terrain and/or other topographic objects such as buildings. In raw LIDAR data, this information is only contained implicitly: the LIDAR beam will not only be reflected at the terrain surface, but on the surface of any object situated on the terrain. If the laser beam is wide enough to illuminate more than one object surface, e.g. in the presence of vegetation, there might even be multiple reflections. A model computed from the raw LIDAR data will be a digital canopy model (DCM) passing through the roofs of the buildings or other objects such as cars, representing the terrain where it is not covered by vegetation, and passing through somewhere between the tops of trees or bushes and the terrain in areas covered by vegetation. Thus, filtering of the raw LIDAR data has been found out to be of crucial importance for DTM generation. In a more general context, one could speak of a classification problem: in order to use LIDAR data for topographic mapping, classification techniques have to be found to separate LIDAR points having been reflected at the surfaces of different objects.

2. LIDAR sensors deliver a 3D point cloud. This might be sufficient for representing the terrain. However, already for the derivation of a high-quality terrain model it is necessary to have vector information about structural lines, especially break lines. On the other hand, buildings are best represented by polyhedral models, their boundaries being described by a set of planar surfaces, by the boundary polygons of these surfaces, and by the mutual topologic relationships of these surfaces. The derivation of such vector descriptions of topographic objects from the original data is another important issue in LIDAR processing.
3. LIDAR data are affected by systematic errors caused by deficiencies in the calibration and by systematic errors of the (LIDAR, INS, and GPS) sensors. With low resolution data height discrepancies in overlapping strips can be recognized resulting in oscillating contour lines in the derived models. Additionally, with high resolution data, the planimetric effects of the systematic errors become evident, too. Thus, the improvement of the georeferencing of LIDAR data is an important topic of research.

It is the goal of this paper to describe the activities of the Institute of Photogrammetry and Remote Sensing at Vienna University of Technology (I.P.F.) in the field of LIDAR processing for topographic mapping. We will especially deal with DTM generation (section 3), automatic building extraction (section 4), and improving the georeferencing of LIDAR data (section 5). Section 2 will give an overview about related work in these research topics, and we will conclude by a summary and an outlook on future work in section 6.

2 RELATED WORK

2.1 DTM Generation from LIDAR Data

For the automated generation of a DTM it is necessary to classify the data obtained by a LIDAR sensor into terrain and off-terrain points, so that there is no influence of the off-terrain points on the terrain model. For this task a lot of different approaches do exist and only a few of them are mentioned in the following.

One group of these algorithms work with image processing techniques in a raster data structure. One of them, presented by Lohmann et al. (2000), is the dual rank filter, a method based on morphological filtering. Von Hansen and Vögtle (1999) have studied a local minimum algorithm and a method called convex/concave surface, whereas an adaptive multi-resolution method is presented by Ziegler et al. (2001).

Another group of algorithms operate on a triangulation of the point cloud data. An adaptive triangular irregular network (TIN) modelling procedure, starting from a sparse TIN which is densified in an iterative process, can be found in (Axelsson, 2000). A different method based on slope based filtering using mathematical morphology working on a TIN structure is presented by Vosselmann and Maas (2001). This filter algorithm defines as threshold for the maximum allowed height difference between two points as a function of the distance between these points in a certain kernel. An extension of this algorithm using a slope adaptive filter to conquer misclassification problems in steep sloped terrain by variable threshold values with respect to the slope of the terrain is presented by Sithole (2001).

A completely different approach for DTM generation from LIDAR founded on active contours based on the theory on active shape models has been developed by Borkowski et al. (1997) and Elmqvist et al. (2001).

2.2 Building Extraction

According to Brenner (2000), building extraction consists of two steps. First, buildings have to be detected in the data, and the approximate building outlines have to be determined. Second, in the regions of interest thus detected, the buildings have to be reconstructed geometrically, which results in 3D polyhedral models of the buildings.

Building detection is based on a classification of LIDAR points according to whether they belong to the terrain, to buildings or to other object classes. Morphological opening filters or rank filters are used to determine a DTM which is subtracted from the digital canopy model (DCM). By applying height thresholds to the height differences, an initial building mask is obtained (Weidner, 1997; Ameri, 2000). This initial classification has to be improved to remove vegetation areas. In (Brunn and Weidner, 1997), this is accomplished by a framework for combining various shape cues in a Bayesian network.

In order to reconstruct the buildings in the regions of interest, parametric primitives can be instantiated and fit to the data if sufficient evidence is found. If 2D ground plans of the buildings are available, the polygon delineating a building in a 2D map can be split into rectangular regions, and in each of the resulting rectangles, the parameters of parametric models can be determined from the DCM. The model achieving the best fit is accepted (Brenner, 2000; Vosselman and Dijkman, 2001).

Building reconstruction can also be based on the detection and grouping of planar patches. Planar patches are found by a segmentation of the DCM. Brenner (2000) gives several methods for DCM segmentation, e.g., the analysis of surface curvature. Ground plans can be used to reduce search space for the estimation of the parameters of adjoining planar patches or to support the precise location of the building outlines (Haala et al., 1998; Brenner, 2000; Vosselman and Dijkman, 2001). Neighbouring planar patches have to be grouped, and the polygons delineating the borders of the planar patches have to be found (Baillard et al., 1999; Moons et al., 1998). These polygons have to be combined in order to obtain consistent building models. A coarse-to-fine strategy can be applied by first searching for the most relevant structures in the data and using refined methods for modeling the buildings in regions not being "explained" sufficiently by the initial models (Vosselman and Dijkman, 2001). The problem of precisely determining the building outlines has been tackled by Weidner (1997) by applying the minimum description length principle for deciding on regularizations.

2.3 Improvement of Georeferencing of LIDAR Data

In LIDAR data sets of low resolutions (e.g., 4 m point distance), the systematic errors caused by deficiencies in the sensor calibration and errors caused by dGPS mainly become evident as height differences in overlapping strips, which might cause contour lines derived from the LIDAR points to oscillate in these regions. A first order error model of LIDAR systems based on the imperfections of the system components has been described by Schenk (2001). He also gives strategies for error recovery. Crombaghs et al. (2002) give a scheme for describing the height errors of digital elevation models (DEMs) from LIDAR and the methods to asses these errors. They distinguish several classes of (random and systematic) errors, depending on the range of their influence, i.e., on the area they will affect: point errors, GPS errors, strip errors, and block errors. Height strip adjustment is a tool for correcting these height errors (Kager and Kraus, 2001). As the resolution of LIDAR data increases, planimetric error components become more and more evident, and these errors have to be considered. This has been performed by 3D strip adjustment compensating for systematic errors such as misalignment of INS, dGPS, and LIDAR sensors and shift and linear drift of orientation positions and attitudes (Burman, 2002; Vosselman and Maas, 2001). The problem of finding homologous surface patches in LIDAR data for strip adjustment has been addressed by Vosselman and Maas (2001) who use a least squares matching (LSM) technique for that purpose. Vosselman (2002) describes the problems encountered with LSM in the cases of height and intensity data, and he describes strategies for avoiding biased estimates of the offset vectors.

3 DTM GENERATION FROM LIDAR DATA

At the I.P.F., an algorithm for the automatic generation of DTMs in forested regions from laser scanner data was developed. This method is based on iterative robust DTM interpolation, and it combines the elimination of off-terrain points and DTM interpolation in one process (Kraus and Pfeifer, 1998). For the generation of a DTM in densely built-up areas, this method has to be modified to work in a hierarchical framework (Pfeifer et al., 2001). With this coarse-to-fine approach it is possible to cope with relatively large areas without terrain points (e.g., large building blocks). Its versatile application possibilities for different data sources are presented in (Briese et al., 2002).

3.1 Robust Linear Prediction

In an iterative process the irregularly distributed LIDAR points are weighted in a way that the modelled surface describes the terrain. The classification of the points in terrain versus off-terrain points is performed by thresholding the discrepancies to the computed surface by user-specified tolerance values.

In a first step, a coarse approximation of the surface is computed taking into account all available LIDAR points. Next, the discrepancies, i.e., the differences of the heights of the original LIDAR points and the interpolated surface at the planimetric positions of the LIDAR points, are computed. The discrepancies are the parameters of a weight

function which is used to assign an individual weight to each point in the subsequent processes. The interpolation of the DTM is repeated, the weights of the LIDAR points being modulated depending on the discrepancies of the most recent iteration. This iterative process is terminated as soon as a stable situation or a maximum number of iterations is reached. Two types of models are used in our algorithm, i.e., the functional model which defines the way the surface is computed, and the stochastic model which is responsible for weighting.

1. **The functional model:** Linear prediction is used for modelling the surface. Using this model, it is possible to compute a smooth surface considering random measurement errors (Kraus, 2000).
2. **The stochastic model:** For the generation of a DTM, high weights must be assigned to terrain points below or on the averaging surface, and low weights have to be assigned to points above the averaging surface. A typical weight function *p(r)* parameterised by the discrepancies *r* for the generation of a DTM from laser scanner data is presented in Figure 2. The weight function we use is not symmetrical, and it is shifted by a value *g*. It has a sharp decline defined by its half-width value *h* and slant *s* for discrepancies greater than its central point (i.e., for off-terrain points above the estimated surface) and no decline for the terrain points. The exclusion of points from the interpolation process is triggered by a threshold *t* derived from a user-specified tolerance for the size of the discrepancies. For a comprehensive description of this algorithm see (Kraus and Pfeifer, 1998).

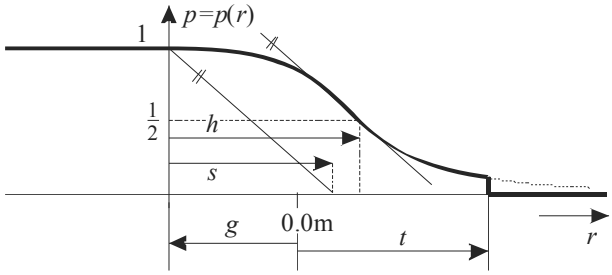

Figure 2. Weight function for the generation of a DTM from laser scanner data.

3.2 Hierarchic Robust Linear Prediction

The method of iterative robust interpolation relies on a more or less random mixture of terrain and off-terrain points. Therefore, this algorithm does not work in large areas without terrain points as they are likely to exist in densely built-up areas. To provide this "good mixture" also in densely built-up areas, robust interpolation has to be applied in a hierarchic way using "data pyramids":

1. Create the data pyramids. This can be achieved by selecting, for instance, the lowest original point in a regular grid mesh.
2. Perform robust interpolation to generate a DTM.
3. Compare the DTM to the data of the next higher resolution and accept points within a certain tolerance band.

Steps 2 and 3 are repeated at each resolution level of the data pyramid. The results of DTM interpolation in the lower resolution levels are used for the computation of the surface in the next higher resolution because only points having passed the thresholding step 3 are considered at that level.

In (Briese, 2001) this strategy has been evaluated for the generation of a high-quality DTM of a test site located in the City of Vienna (2.5 km²) using three data pyramid levels (5 m, 2 m and 0.5 m). A few intermediate and the final results of this DTM generation process are presented in Figures 3a-b. Further details about hierarchical robust interpolation, its implementation in the software package SCOP++, and the results of some further examples can be found in (Pfeifer et al., 2001).

3.3 Improvement of the Geomorphologic Quality of LIDAR DTMs

LIDAR sensors offering a high point density, allow to generate very detailed DTMs with very small grid sizes. However, terrain models with high geo-morphological quality excel in the inclusion of structure lines, especially

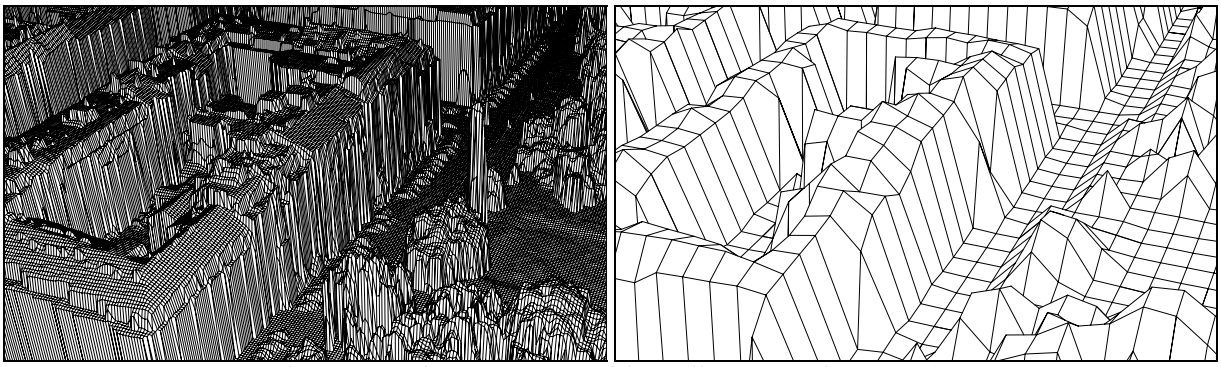

Figure 3a. Left: DCM computed from all LIDAR points (0.5 m).
Right: DCM at the lowest resolution (5 m).

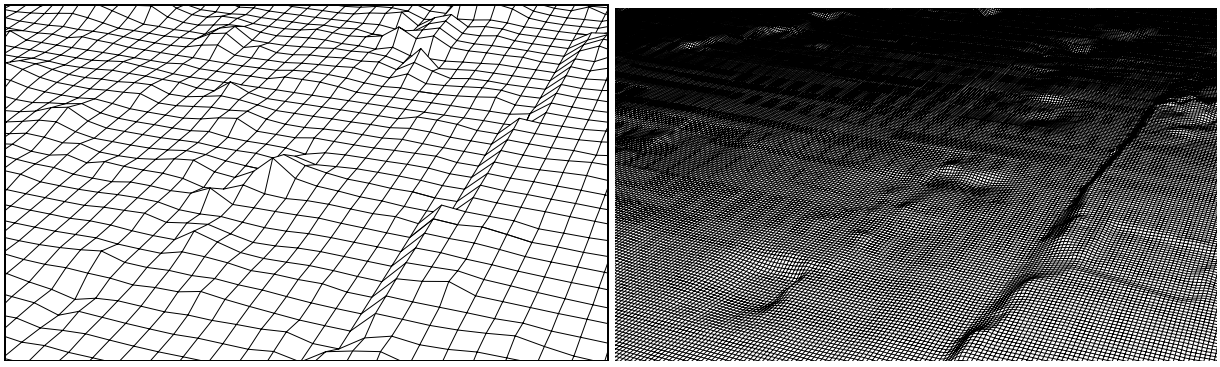

Figure 3b. Left: DTM at the lowest resolution (5 m).
Right: Final DTM (0.5 m; here: 1.0 m for better readability).

break lines. To generate these models from LIDAR data, methods for deriving information about structural lines are required. The first method to be presented here is based on a simulation of rain fall over the preliminary DTM and a water flow analysis, whereas the second method uses approximate planimetric positions of break lines to derive 3D break lines from the LIDAR point cloud. With this additional vector information, a hybrid DTM integrating raster and vector data can be generated. Random errors should be considered for the measured point cloud data as well as for the generated vector information within the surface modelling process (Kraus, 2000).

3.3.1 Water Flow Analysis

The first developed method in break line detection is based on a water flow analysis applied to a DTM (Rieger, 1992). The assumption behind this method is that the terrain surface is formed by the process of water transport. Spurious pits in the DTM are just caused by the interpolation process applied to original data of insufficient resolution and, therefore, must be removed. As a result of this algorithm, it is possible to extract 3D river lines which show the highest amount of water transport. These lines are included in the following interpolation process as "break lines". The resulting hybrid model has no (artificial) pits anymore. Gaisky (2000) applied this method to a digital terrain model derived from LIDAR data. This method shows reasonable results in certain areas where the terrain surface is the result of the process of water transport. This method has problems in flat regions where the water flow cannot be determined well and in areas with an artificial terrain surface.

3.3.2 Derivation of Break lines

The method - already presented in (Kraus and Pfeifer, 2001) - requires the planimetric positions of the break lines to be approximately known. This starting position can be provided manually or by image processing tools, e.g. (Rieger et al., 1999) and (Brügelmann, 2000).

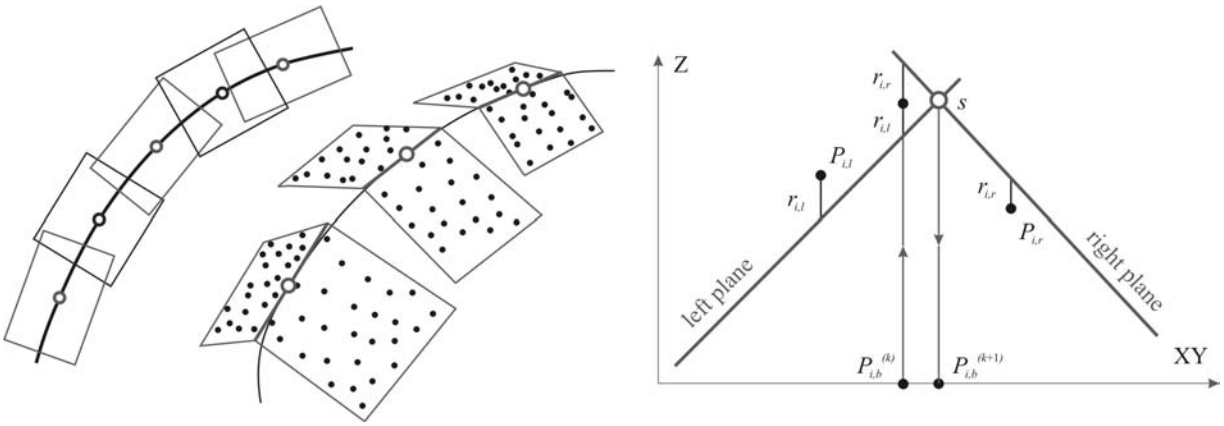

Figure 4. Left and middle: overlapping segments with plane pairs along a break line in a ground plan and in axonometric view. Right: one plane pair, the intersection line *s* appears as a point (Kraus and Pfeifer, 2001).

In our method, a break line is determined in 3D by intersection of local object surface patches, thus also refining its planimetric position (see also Figure 4). First, the break line is split into overlapping segments, and in each of these segments, the initial position of the break line is used to classify the laser scanner data in its surrounding into the groups 'left' and 'right'. Then, for each segment a pair of planes, one approximating the terrain on the left and the other doing so on the right side of the break line, is determined by least squares adjustment. The resulting planes intersect in the straight line *s* which can be used as refined approximation of the break line segment for a further iteration. After a certain number of iterations the result of this process is the refined 3D straight line segment of intersection *s*. A 3D point is computed in the centre of each segment *s*. Finally, the 3D break line is approximated by a spline function so that these 3D points are its vertices and the straight line segments *s* are its tangents in these points. An example for the results of this process can be found in Figure 5 which also allows a view on the data structure of the resulting hybrid DTM.

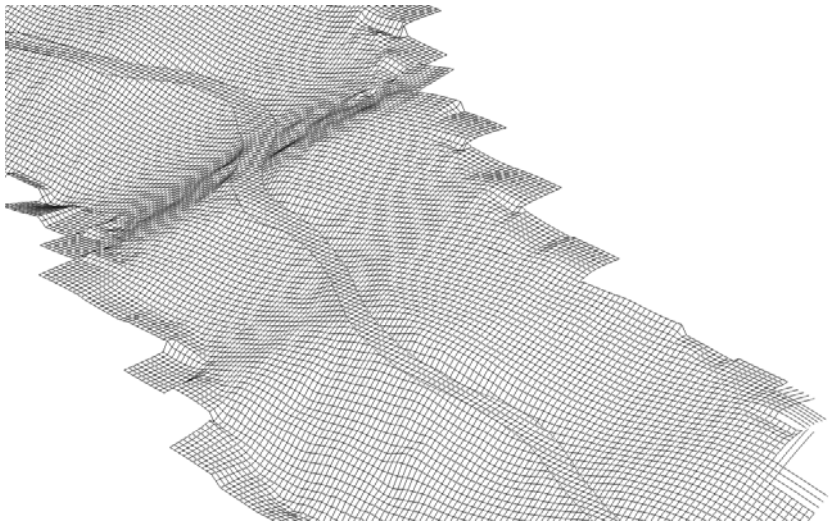

Figure 5. Perspective view of the DTM with automatically measured break lines (Kraus and Pfeifer, 2001).

These break lines are also a very important data source for the improvement of the DTM generation process. The classification of LIDAR data in terrain and off-terrain points is difficult in areas where the terrain surface has discontinuities in the first derivates. Therefore, modelling these discontinuities by break lines and integrating these lines into the classification process leads to much more reliable results. The first test using break lines within the hierarchic robust interpolation technique (the break lines are treated as free of gross errors) showed that an

improvement in the height accuracy is possible. The r.m.s. error of the discrepancies with respect to check points measured tachymetrically on the break line was reduced from ±29 cm to ±19 cm. Additionally, the systematic error (in the area of the break line, the LIDAR DTM was lower than the check points) improved from 24 cm to 15 cm.

4 BUILDING EXTRACTION FROM LIDAR DATA

At the I.P.F., a method for the automatic generation of polyhedral building models from high-resolution LIDAR data working without additional information such as 2D maps is being developed. With respect to building detection, this method relies on the results of hierarchic robust interpolation (cf. section 3.2). In the detected building regions, planar roof patches, their bounding polygons, and their neighbourhood relations are extracted. Grouping of neighbouring planes has not yet been implemented. The examples presented in this section again were computed using data from the I.P.F.'s test site in the City of Vienna.

4.1 Detection of Building Regions

Two digital elevation models are derived by interpolation: a DTM is computed from the points classified as "terrain points", whereas a DCM is computed from all points without smoothing (Figure 6a). An initial building mask is created by thresholding the height differences between the DCM and the DTM (Figure 6b). A morphological opening filter using a small square structural element is applied to the initial building mask in order to erase small elongated objects and to separate regions just bridged by a thin line of pixels. The initial building regions are obtained by a connected component analysis of the resulting image. At this instance, regions smaller than a minimum and regions at the border of the DCM are discarded (Figure 6c).

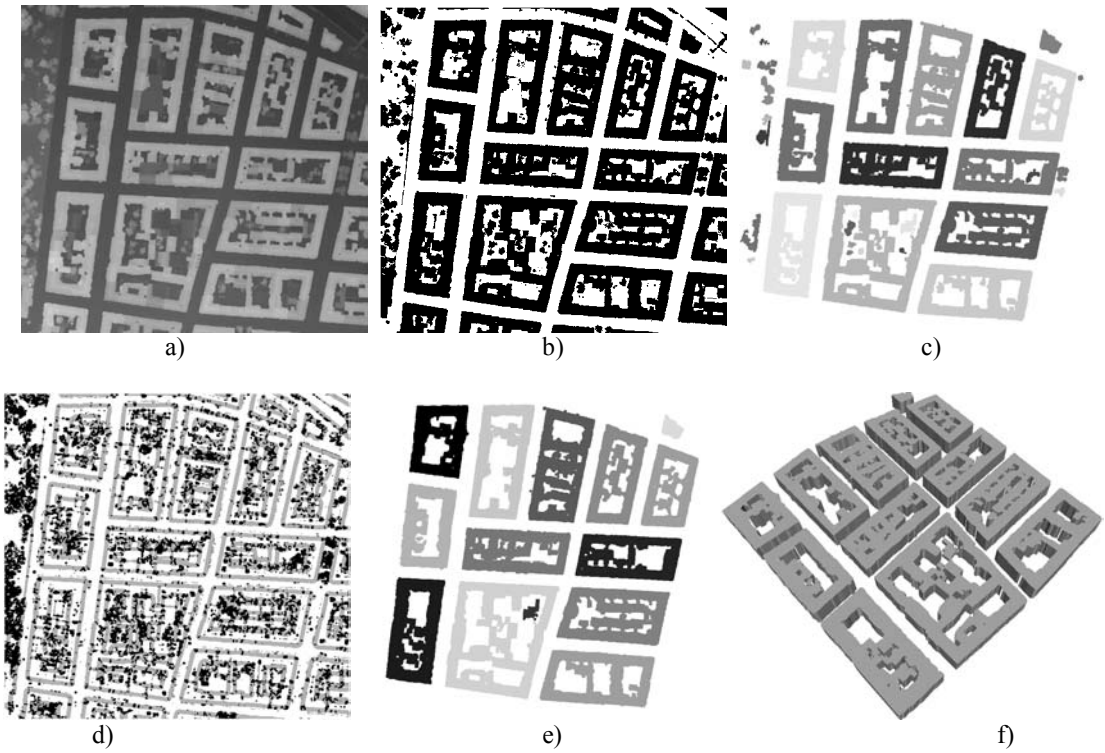

Figure 6. Building detection in a test site in the City of Vienna.
a) DCM; grid width: 0.5 m; extent: 410 x 435 m^2. b) Initial building mask (Δh_{min}=3.5m).
c) Initial building label image before evaluating terrain roughness area (area threshold: 40 m^2).
d) Results of texture classification. Point-like pixels are displayed in black.
e) Final building label image. 14 building regions have been detected.
f) Visualization of block models created from the boundaries of the building regions from Figure 6e.

Some of the remaining regions in Figure 6c still correspond to groups of trees. These regions can be eliminated by evaluating a "terrain roughness" criterion. In (Fuchs, 1998), a method for polymorphic feature extraction is described that aims at a classification of texture as being homogeneous, linear, or point-like, by an analysis of the first derivatives of a digital image. This method is applied to the first derivatives of the DCM (Figure 6d). Initial "building regions" containing more than 50% of pixels classified as being "point-like" (pixels in a neighbourhood of great, but anisotropic variations of the surface normals) are likely to contain vegetation, and they are eliminated.

The terrain roughness criterion is very efficient in classifying isolated vegetation regions, but it cannot find vegetation areas that are still connected to buildings. In a final stage of analysis, we try to eliminate such areas. First, areas just connected by small bridges are separated, which results in new initial building regions, and then the terrain roughness criterion is evaluated again. Pixels being in regions now classified as containing vegetation are erased in the initial building label image. Thus, in vegetation areas originally connected to buildings, only the border pixels remain classified as "building pixels". Again, morphological opening helps to erase these border pixels. The resulting building label image only contains a small percentage of erroneously classified pixels in some backyards (Figure 6e).

At a very coarse level of detail, a 3D city model can be derived by creating block models from the boundary polygons of the building regions using the average building heights computed from the DCM. An example for such a city model with a height accuracy of about ±5 m is shown in Figure 6f.

4.2 Reconstruction of Polyhedral Models

4.2.1 Generation of initial 3D planar segments: To start with model generation, initial 3D planar segments, their geometrical parameters, and their initial border polygons have to be found in the regions of interest. This is achieved by generating a "segment label image" defined in object space with an appropriate grid width. Each pixel of that image is assigned the label of the planar segment it belongs to.

The framework for polymorphic feature extraction (Fuchs, 1998) is applied to the first derivatives of the DCM for the generation of planar segments. Pixels classified as being homogeneous are surrounded by pixels having similar components of the normal vector, i.e., they are in a region containing co-planar points (Brunn and Weidner, 1997). The binary image of the homogeneous pixels is used for further processing (Figure 7a). By applying a connected component analysis to this binary image, planar patches should be detectable. However, due to classification errors, especially at the intersections of roof planes which are almost horizontal, the regions thus detected often turn out to be too large. In order to avoid these errors, an iterative strategy is applied for the generation of planar patches:

1. The binary image of homogeneous pixels is morphologically opened using a square structural element before applying the connected component analysis.
2. The geometric parameters of the planar patches thus detected are derived along with their r.m.s. errors from all points inside these patches.
3. The patches with the best fit, i.e., those with r.m.s. errors better than a certain threshold are considered to be seed regions for region growing. In this way, the most relevant and best fitting planes are extracted from the DCM.
4. The plane parameters are updated, and the pixels already being assigned to a planar patch are erased in the binary image. The connected component analysis is repeated, and the parameters of the new planar patches are evaluated.

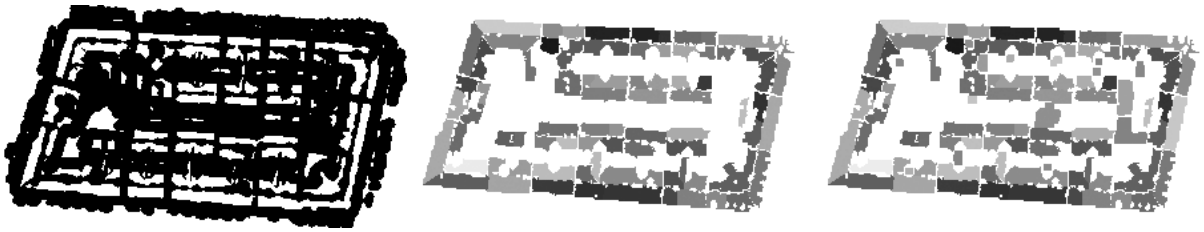

a b c

Figure 7. a) Pixels classified as "homogeneous" (white) for one of the building regions in Figure 6e.
b) Planar patches obtained by iteratively applying region growing.
c) Final segment label image for one of the building regions in Figure 6e.

Steps 1 to 4 are repeated with a decreasing size of the structural element for morphological opening. Thus, smaller and smaller initial regions are found, and by only allowing well-fitting planes to grow, it is possible to split the regions corresponding to more than one roof plane, because the r.m.s. error of the planar fit is a good indicator for the occurrence of such situations. Figure 7b shows the planar patches extracted in one of the building regions from Figure 6e.

A further analysis has to detect planes which cover too small an area for resulting in pixels classified as being homogeneous. We search for regions not being consistent with the planar regions detected so far. We look for connected components of still unclassified pixels in order to create additional candidates for planar patches (Figure 7c). The r.m.s. errors of planar adjustment varies between ±5 cm and ±20 cm for the segments corresponding to the "homogeneous" points. The segments having a r.m.s. error larger than ±15 cm possibly still correspond to more than one roof plane. In the planar regions created by the analysis of the originally inconsistent points, the r.m.s. errors vary between ±25 cm and ±5 m. Some of these regions correspond to trees, and other regions still correspond to more than one roof plane. In the future, a further analysis will split these regions into smaller ones corresponding to even smaller planes in object space. This can be accomplished, e.g., by a height segmentation of the DCM in these regions. Table 1 shows the distribution of the r.m.s. errors of the planar fit.

r.m.s. error [m]	Regions	Pixels [%]
0.00 - 0.10	574	75.0
0.10 - 0.20	229	18.1
0.20 - 0.50	26	0.9
0.50 - 1.00	10	0.2
1.00 - 3.00	56	3.1
>=3.00	51	2.7

Table 1. Distribution of the r.m.s. errors of the planar fit. Regions: number of planar regions in the respective range of r.m.s. errors. Pixels: percentage of pixels in these regions compared to the number of all pixels in all planar regions. 68% of the pixels in the building candidate regions are classified as belonging to a planar region.

4.2.2 Grouping planar segments to create polyhedral models: To derive the neighbourhood relations of the planar segments, a Voronoi diagram based on a distance transformation of the segment label image has to be created (Ameri, 2000): each pixel inside the region of interest not yet assigned to a planar segment is assigned to the nearest segment. The distances of pixels from the nearest segment are computed by using a 3-4 chamfer mask (Figure 8a). From the Voronoi diagram, the neighbourhood relations of the planar segments are derived, and the borders of the Voronoi regions can be extracted as the first estimates for the border polygons of the planar segments (Figure 8b).

a b

Figure 8. a) A Voronoi diagram of the label image in Figure 7c.
b) The roof polygons of the building in a) back-projected to an aerial image.

Neighbouring planar segments have to be grouped. There are three possibilities for the relations of two neighbouring planes (Baillard et al., 1999). First, they might be co-planar, which is found out by a statistical test applied to the plane parameters. In this case, they have to be merged. Second, two neighbouring planes might intersect consistently, which is the case if the intersection line is close to the initial boundary. In this case, the intersection line has to be computed, and both region boundaries have to be updated to contain the intersection line. Third, if the planes do not intersect in a consistent way, there is a step edge, and a vertical wall has to be inserted at the border of

these segments. After grouping neighbouring planes, the bounding polygons of all enhanced planar regions have to be completed. (Moons et al., 1998) give a method for doing so and for regularizing the shape of these polygons at building corners. Finally, the planar polygons have to be combined to form a polyhedral model, and vertical walls as well as a floor have to be added to the model.

The tools for grouping planes and for computing intersections and the positions of step edges have not yet been implemented. Figure 9 shows a VRML visualization of a 3D model created from intersecting vertical prisms bounded by the borders of the Voronoi regions with the respective 3D roof planes. The structure of the roofs is correctly resembled, but the intersection lines of neighbouring roof planes are not yet computed correctly. However, the visualization shows the high potential of the method for generating roof planes from LIDAR data.

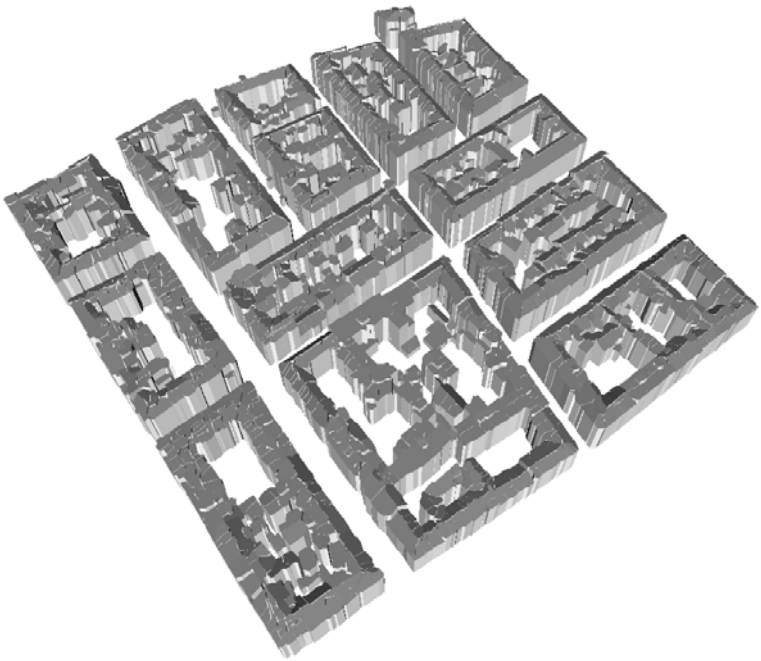

Figure 9. VRML visualization of a model created from the boundary polygons of the Voronoi diagram in Figure 8a.

5 IMPROVEMENT OF GEOREFERENCING OF LIDAR DATA

In his error model of LIDAR systems, Schenk (2001) described the following sources for systematic errors and bounds of these errors:

- Systematic errors in the laser scanner system: index errors of the laser scanner system of up to 0.02° and scan angle errors as well as errors of the scan plane alignment of up to 0.03° will cause partly non-linear errors in the 3D positions of LIDAR points of up to 60 cm at 1000 m flying height.
- Mounting errors of both the GPS and the INS systems: after in-flight calibration, there remains a systematic mounting error of up to 0.01° between the GPS and INS sensors.
- Systematic GPS errors: the on-the-fly-initialisation for solving the GPS phase ambiguities is possible for fast moving objects with an r.m.s. error of about 10 cm; usually, the neighbouring precision of dGPS is better by one order of magnitude. Some displacement might also be caused by system failure or system instabilities, e.g., by the change of the set of available GPS satellites during a strip; however, INS data helps to bridge such critical gaps.
- Systematic INS errors: these errors might reach 0.01°. Errors of INS attitude also introduce some torsion of the laser scanner strips inducing errors in height and planimetry on both borders of the strip. Equally, INS attitudes have a high neighbouring precision based on the gyros used; nevertheless, they show drifting phenomena.
- Systematic errors caused by badly known geoid normals: the form of the geoid is not sufficiently (up to some few cm) known in many regions. Schenk (2001) estimates the maximum deflection of the vertical to be 0.017°.

We suggest to use of more than one GPS ground reference stations surrounding the area of interest. Knowing the ground survey coordinates of all these ground reference stations, this can be used to improve the transformation parameters between the national surveying co-ordinate system and the GPS co-ordinate system, e.g., WGS 84, and it eliminates the (unknown) linear portion of the geoid's undulation. The undulations of higher degree remain; they might be neglected for the usually relative small extent of practical projects. Some of the GPS ground reference stations may be replaced by ground reference points (better: reference features) that can be "identified" somehow in the point clouds of the laser scanner strips. In photogrammetric terminology, we usually call those reference points control points (Kager and Kraus, 2001). In order to compensate for the other systematic errors in the above list, three strategies can be followed depending on the resolution of the LIDAR data:

1. **Simultaneous height adjustment of LIDAR strips**: This method can be applied to correct for systematic errors in low-resolution data. The coefficients of correction polynomials are determined using the LIDAR points in (horizontal) homologous patches in different strips. As stated above, control patches (patches of known height) can be used, too.
2. **3D strip adjustment**: The method of height adjustment can be expanded to 3D strip adjustment using correction polynomials for the planimetric co-ordinates, too. For that purpose, the tie patches must no longer be exclusively horizontal. This means that it is necessary to extract 3D features in different strips. Control features can be used if the results are to be obtained in a national reference co-ordinate system.
3. **LIDAR correction by modelling the flying path and the sensor attitudes**: A more general technique aims at using raw GPS, INS, and laser scanner data synchronized by a time stamp to directly model the flight paths, the sensor attitudes, and the systematic errors of the individual sensors. Again, 3D features have to be extracted in different strips, and it is possible to use control features if the results are to be obtained in a national reference co-ordinate system.

In the following sections, we will describe methods following strategies 1 and 3 developed at the I.P.F.

5.1 Simultaneous Height Adjustment of LIDAR Strips

The principles of the simultaneous height fitting of all laser scanner strips can be found in Figure 10. XY-positions are defined in a scheme which is – on the one hand – related to the strip borders and – on the other hand – controllable from outside. This control is performed by selection of an interval of the profiles crossing the strips and of a point interval inside the profiles. The first distance is measured (more or less) along the flying track, the second one perpendicular to the first one. Points are preferably chosen in areas of much overlap. Starting from every scheme point, a search for suitable homologous patches is done; 'suitable' means that there is as few vegetation as possible and the area is as horizontal as possible, 'homologous' means that the patch has the same position in every involved strip, 'patch' means a rectangular area (externally controllable) of e.g. 20 points. The set of surfaces inside a patch region is approximated by a (tilted) plane:

$$v_{t,s,p} = a_t \cdot \left(\overline{X}_{t,s,p} - X_t\right) + b_t \cdot \left(\overline{Y}_{t,s,p} - Y_t\right) + Z_t + dZ_s(c_{sij}, X_{ts}, Y_{ts}) - \overline{Z}_{t,s,p} \qquad (1)$$

$\mathbf{P}_{t,s} = \overline{X}_{t,s,p}, \overline{Y}_{t,s,p}, \overline{Z}_{t,s,p}$	. . .	point ***P*** in patch *t* of strip *s*; "raw" co-ordinates
X_t, Y_t	. . .	centre of patch *t*; constant; modulated as given below
Z_t	. . .	unknown height of the patch *t*
a_t, b_t	. . .	unknown tilts of patch *t*
X_{ts}, Y_{ts}	. . .	centre of patch *t* in strip co-ordinates of strip *s*: $X_s = X_t - X_{0s}$, $Y_s = Y_t - Y_{0s}$
$dZ_s(c_{sij},X_{ts},Y_{ts})$	. . .	correction polynomial of strip *s*
c_{sij}	. . .	unknown polynomial coefficients of the correction polynomial
$v_{t,s,p}$	. . .	height residuals for point ***P*** in the least squares adjustment

The search for (X_t, Y_t) follows a spiral pattern in the surrounding of the scheme point until certain quality criteria are satisfied. For instance, freedom of vegetation or other disturbances is judged by a tolerance of the r.m.s. error of the above adjustment problem. Horizontality can be judged on a_t, b_t. The patch size is chosen in accordance with the geometry of the scanner (point density along and across the strip) to contain about 20 to 150 points per strip overlay. Planimetric discrepancies between the strips don't play a remarkable role as long as the terrain is flat enough.

Subsequently, the heights $\overline{Z}_{t,s,p}$ of points $\boldsymbol{P}_{t,s}$ are used as observations in block adjustment. Additional observations are fictitious observations of these points' distances from the adjusting planes and, in case of such information being available, the heights Z_t of control patches. The unknowns are the parameters (a_t, b_t, Z_t) of the (tie and control) patches, the object co-ordinates of the LIDAR points, and the coefficients c_{sij} of the correction polynomials. The details of the block adjustment with the ORIENT software are described in (Kager and Kraus, 2001).

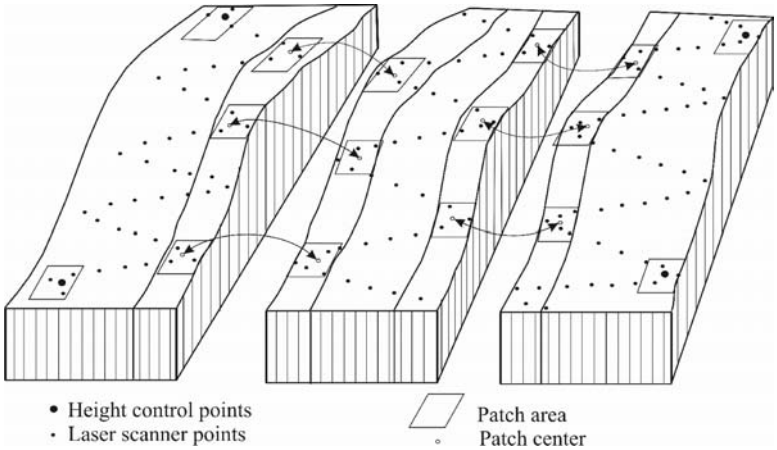

Figure 10. Principle of height block adjustment with laser scanner strips.

For a pilot project with the "Bundesanstalt für Gewässerkunde" in Koblenz (Germany), the "German Federal Institute of Hydrology" we had no suitable control points available. Thus, an absolute fit to the national ground survey co-ordinate system was not possible (no datum given). Nevertheless, the aim of the project was a homogenisation of the block of 56 strips by diminution of the discrepancies between overlapping strips. The scheme points for the automatic measurement of tie points were arranged in profiles perpendicular to the main direction of the strips with profile distances of 1000m. (Experiments with smaller profile distances yield approximately the same results.) The height discrepancies between the laser scanner strips prior to adjustment were determined for 1495 patches. The r.m.s. error was ±10.7 cm. By the block adjustment we got a reduction by a factor of 2. In a second pilot project – in the framework of European Union INTERREG projects – we obtained an improvement by the block adjustment by a factor of 2.5.

5.2 LIDAR Correction by Modelling the Flight Path and the Sensor Attitudes

In this section we want to present a parametric procedure for LIDAR correction. This method requires the following data to be available:

1. GPS co-ordinates for points along the flight path in a co-ordinate system related to GPS and a time stamp for each of the GPS points
2. Direct observations for the rotational angles $\vartheta = (Roll, Pitch, Yaw)^T$ delivered by the INS and a time stamp for each observed triple of rotational angles
3. The laser observations, i.e., the distance d and the deflection angle τ_i for each of the LIDAR points and a time stamp for each of these LIDAR points for synchronisation with GPS and INS.
4. Some 3D tie features identified in the overlapping areas of the LIDAR strips. Some of these features might be control features.

The LIDAR observations are taken in the LIDAR co-ordinate system (x_s,y_s,z_s) which is centred at the laser firing point, the x_s-axis being parallel to the flying direction, and the z_s-axis is parallel to the line given by $\tau_i = 0$, but pointing upwards (Figure 11). The actual observations are polar co-ordinates: a directional angle α (e.g., with $\alpha = 100^{gon}$ if the laser beam is deflected in a plane orthogonal to the x_s -axis), the zenith angle ζ with $\zeta = 200^{gon} - \tau_i$, and the distance d. The LIDAR co-ordinates can be computed from these polar observations from equation 2:

$$\mathbf{x_s} = \begin{pmatrix} x_s \\ y_s \\ z_s \end{pmatrix} = d \cdot \begin{pmatrix} \cos(\alpha) \cdot \sin(\zeta) \\ \sin(\alpha) \cdot \sin(\zeta) \\ \cos(\zeta) \end{pmatrix} = d \cdot \begin{pmatrix} 0 \\ \sin(\tau_i) \\ -\cos(\tau_i) \end{pmatrix} \tag{2}$$

The rightmost portion of equation 2 is only valid under the assumptions cited above ($\alpha = 100^{gon}$, $\zeta = 200^{gon} - \tau_l$,). The relationship between the LIDAR co-ordinate system and the world co-ordinate system (X_w, Y_w, Z_w) at the time t is given by a spatial congruency transformation (equation 3):

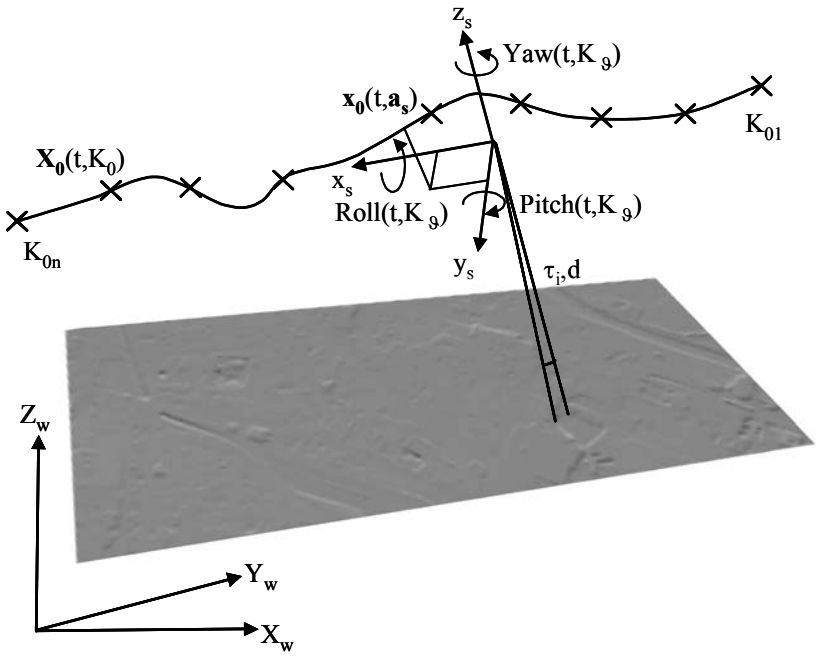

Figure 11. A LIDAR strip and the relations between the LIDAR and the world co-ordinate systems.

$$\mathbf{x}_S - \mathbf{x_0}(t, \mathbf{a_s}) = \mathbf{R}^T \left[\vartheta(t, \mathbf{K}_\vartheta)\right] \cdot \left[\mathbf{X} - \mathbf{X_0}(t, \mathbf{K_0})\right] \tag{3}$$

$\mathbf{X} = (X_w, Y_w, Z_w)^T$	. . .	the object point in the world co-ordinate system
$\mathbf{x_s} = (x_s, y_s, z_s)^T$	. . .	the point in the LIDAR co-ordinate system according to equation 2
$\mathbf{x_0}(t, \mathbf{a_s})$	. . .	the "inner reference point" in the LIDAR co-ordinate system
$\mathbf{R} = \mathbf{R}[\vartheta(t, \mathbf{K}_\vartheta)]$	. . .	a rotational matrix depending on the rotational angles ϑ at the time t; $\mathbf{R}^T$ means $\mathbf{R}$ transposed
$\mathbf{X_0}(t, \mathbf{K_0})$	. . .	the position of the GPS antenna in the world co-ordinate system at time t (Figure 11).

In equation 3, the flight path of the GPS antenna $\mathbf{X_0}(t, \mathbf{K_0})$ is modelled by a 3D cubic spline depending on time t and the flight path spline nodes $\mathbf{K_0}$. In a similar way, the rotational angles $\vartheta(t, \mathbf{K}_\vartheta)$ are modelled by another 3D cubic spline depending on time t and the rotational spline nodes $\mathbf{K}_\vartheta$. Thus, the flight path and the sensor attitudes are modelled by a 6-dimensional orientation spline. The same model for the flight path and sensor attitudes is used in the I.P.F.'s bundle adjustment system ORIENT (ORIENT, 2000) for airborne optical line scanners (Ries et al., 2000). The principle of using "orientation splines" in this context was first presented by Forkert et al. (1997). The co-ordinates of the inner reference point $\mathbf{x_0}(t, \mathbf{a_s})$ consists of a constant offset describing the offset of the GPS antenna and time-dependent components which are meant to correct for systematic errors in the LIDAR system such as the scan angle error. The antenna offset and the parameters of these time-dependent functions denoted by the vector of additional scanner parameters $\mathbf{a_s}$. Note that in equation 3, the actual observations $(\alpha = 100^{gon}, \zeta = 200^{gon} - \tau_l,$

d) are only contained in an implicit form in the components of $\mathbf{x_s}$. Kraus (1997) gives a method for generating explicit polar observation equations from the spatial congruency transformation.

The GPS points $\mathbf{x_{GPS}}$ are available in the GPS co-ordinate system which is also related to the world co-ordinate system by a spatial congruency transformation (equation 4). They are observations for the flight path spline $\mathbf{X_0}(t,\mathbf{K_0})$:

$$\mathbf{x_{GPS}} - \mathbf{x_{0GPS}}\left(t,\mathbf{a_{GPS}}\right) = \mathbf{R}^T\left(\vartheta_{GPS}\right)\cdot\left[\mathbf{X_0}\left(t,\mathbf{K_0}\right) - \mathbf{X_{0GPS}}\right] \tag{4}$$

In equation 4, the role of the object point is taken over by the flight path spline $\mathbf{X_0}(t,\mathbf{K_0})$; there is an unknown shift vector $\mathbf{X_{0GPS}}$ and an unknown set of rotational angles $\boldsymbol{\vartheta}_{\mathbf{GPS}}$. Again, an interior reduction point $\mathbf{x_{0GPS}}(t,\mathbf{a_{GPS}})$ is deducted from the observed point $\mathbf{x_{GPS}}$ to correct for systematic shift and drift errors. The correction functions are polynomials parameterised by the additional GPS parameters $\mathbf{a_{GPS}}$. There might be a constant offset describing a systematic shift and time-dependent components for modelling the fine drift. In ORIENT, it is up to the user to decide about the specific subset of additional parameters to be used for a certain project. In addition, it is possible to assign different sets of additional parameters to different groups of LIDAR strips (e.g., one set of parameters per flying direction in meandering flights), to different strips, or even to different strip sections.

In a similar way as GPS co-ordinates, the observed INS angles $\boldsymbol{\vartheta}_{\mathbf{INS}}$ are considered to be direct observations for the rotational spline $\boldsymbol{\vartheta}(t,\mathbf{K}_{\boldsymbol{\vartheta}})$, and there is a "reduction point" $\boldsymbol{\vartheta}_{\mathbf{oINS}}(t,\mathbf{a_{INS}})$ consisting of a constant offset (describing the angular offset between the INS from the LIDAR co-ordinate systems) and time-dependent functions modelling fine drift of the INS. The correction functions are parameterised by additional INS parameters $\mathbf{a_{INS}}$. Again, it is possible to assign different sets of additional parameters to different groups of LIDAR strips, to individual LIDAR strips, or to strip sections.

$$\vartheta_{\mathbf{INS}} - \vartheta_{\mathbf{oINS}}\left(t,\mathbf{a_{INS}}\right) = \vartheta\left(t,\mathbf{K}_{\vartheta}\right) \tag{5}$$

In order to correct for the systematic errors, homologous 3D features have to be found in the LIDAR data (Vosselman, 2001). The following observations are used in least squares adjustment:

- The polar observations *(*e.g., $\alpha = 100^{gon}$, $\zeta = 200^{gon} - \tau_l$, *d)* of the LIDAR points in the homologous (tie or control) features in different strips. They are related to the world co-ordinate system by equation 3 (modified to make the observations explicit by considering equation 2)
- Observations of the distances of these LIDAR points from the adjusted (tie or control) patch in object space. Of course, as the LIDAR points are situated in these patches, these distances are observed to be 0.
- The GPS co-ordinates linked to the world co-ordinate system by equation 4.
- The INS angles linked to the rotational splines by equation 5.
- The parameters of control features.

These observations are used to compute the following unknowns:

- The object co-ordinates of the LIDAR points
- The nodes $\mathbf{K_0}$ of the flight path spline $\mathbf{X_0}(t,\mathbf{K_0})$
- The nodes $\mathbf{K}_{\boldsymbol{\vartheta}}$ of the rotational spline $\boldsymbol{\vartheta}(t,\mathbf{K}_{\boldsymbol{\vartheta}})$
- The parameters of the patches
- The transformation parameters $\mathbf{X_{0GPS}}$ and $\boldsymbol{\vartheta}_{\mathbf{GPS}}$ between the GPS and the world co-ordinate systems.
- The unknown additional parameters for correcting the systematic errors:
  - The additional scanner parameters $\mathbf{a_s}$ for modelling systematic errors in the LIDAR system, including the GPS antenna offset
  - The additional GPS parameters $\mathbf{a_{GPS}}$ for modelling systematic shifts and drifts in the GPS system
  - The additional INS parameters $\mathbf{a_{INS}}$ for modelling systematic shifts and drifts in the INS.

Note again that there might be different sets of additional parameters to be determined for different strips. This has been shown to be very useful for correcting systematic errors with problems in the GPS observations of a specific

optical line scanner strip by Ries et al. (2002). The model presented here is currently improved to eliminate the great number of unknown spline nodes, and the mathematical model for the correction functions in the LIDAR system are worked out. The method does not correct for misalignment errors between GPS and INS. This is not a principal problem of the technique, but there is not yet an emphasis on correcting for these errors because the data required for that purpose ("uncorrected" GPS data at the frequency of differential GPS) are not available, and the INS data are also already smoothed. A test project using "raw" data in the sense described above is currently being worked out at the I.P.F.

6 SUMMARY AND OUTLOOK

We have presented the activities of the I.P.F. in the field of LIDAR processing. LIDAR has turned out to be an important data source, because it offers a high potential for automation of the tasks related to topographic modelling. Models of the terrain or topographic objects can be derived from LIDAR data in a relatively short turnout time.
We have addressed the problem of DTM generation. Our technique for hierarchic robust interpolation has been shown to give very good results even in densely built-up areas. Problems may arise in alpine regions or in regions of rough terrain, because there the method might filter too much. In the future, we will try to include intensity and/or colour information into the filtering process to predict areas where filtering has to be applied due to vegetation, an a priori information which could be used in the interpolation process to assign different a priori weights to the LIDAR points. The method of 3D break line detection is further improved in a research project so that the local planes are replaced by surfaces of a higher order, and the estimation of the local plane parameters and the adjustment of the 3D spline are integrated.

We have further shown the preliminary results of our method for building extraction. These results are very encouraging, and we are currently about to implement the modules still missing, i.e., the tools for grouping the initial planar patches. Our test results have shown that a very high level of detail could be achieved if the resolution of the LIDAR data were higher than the one used in our test project. Instead of using LIDAR data of a higher resolution, it is also possible to combine LIDAR data with aerial images of a higher resolution to improve the results of building extraction, especially at the building outlines. This is also currently investigated at the I.P.F.

Finally, we have presented two methods for improving the geocoding of LIDAR data using "raw" data. The method for height correction by simultaneous fitting of strips has given good results for a test project in low-resolution data. Especially for high-resolution data, a technique for 3D correction is necessary. We have presented an adjustment technique for LIDAR data based on modelling the flight paths and sensor attitudes by splines and correcting for systematic errors by additional parameters. Originally, this adjustment technique was developed for optical line scanners, where it has been shown to be well-suited for handling problematic situations. Currently, it is improved to reduce the number of unknowns in the adjustment process, and a test project using original (LIDAR, GPS, and INS) data is currently worked out.

REFERENCES

Ameri, B., 2000: Automatic Recognition and 3D Reconstruction of Buildings from Digital Imagery. PhD Thesis, Institute of Photogrammetry, Stuttgart University, DGK-C 526.

Axelsson, P., 2000. DEM generation from laser scanner data using adaptive TIN models. International Archives of Photogrammetry and Remote Sensing, Vol. XXXIII, Part B4, Amsterdam, Netherlands.

Baillard, C., Schmid, C., Zisserman, A., Fitzgibbon, A, 1999: Automatic line matching and 3D reconstruction of buildings from multiple views. IAPRS 32 (3-2W5), pp. 69-80.

Borkowski, A., Burghardt, D., Meier, S., 1997. Zur optimalen Approximation von Höhenprofilen. Österreichische Zeitschrift für Vermessung und Geoinformation (VGI), 85(4), pp. 281 - 285.

Brenner, C., 2000: Dreidimensionale Gebäuderekonstrutkion aus digitalen Oberflächenmodellen und Grundrissen. PhD Thesis, Institute of Photogrammetry, Stuttgart University, DGK-C 530.

Briese, Ch., 2001: Digitale Modelle aus Laser-Scanner-Daten in städtischen Gebieten. Diploma Thesis, Inst. of Photogrammetry and Remote Sensing, Vienna University of Technology.

Briese, Ch., Pfeifer, N., Dorninger, P, 2002. Applications of the Robust Interpolation for DTM determination. Symposium der ISPRS-Comm. III, Graz. International Archives of Photogrammetry and Remote Sensing, Volume XXXIV / 3A, pp. 55 - 61.

Brügelmann, R., 2000. Automatic breakline detection from airborne laser range data. International Archives of Photogrammetry and Remote Sensing, Vol. XXXIII, Part B3, pages 109-115, Amsterdamm, Netherlands.

Brunn, A., Weidner, U., 1997: Extracting Buildings from Digital Surface Models. IAPRS 32 (3-4W2), pp. 27-34.

Burman, H., 2002: Laser strip adjustment for data calibration and verification. IAPRS 34 (3A), pp. 67-72.

Crombaghs, M., Elberink, S.O., Brügelmann, R., de Min, E., 2002: Assessing height precision of laser altimetry DEMs. IAPRS 34 (3A), pp. 85-90.

Elmqvist, M., Jungert, E., Lantz, F., Persson, A., Södermann, U., 2001. Terrain Modelling and analysis using laser scanner data. International Archives of Photogrammetry and Remote Sensing, Volume XXXIV-3/W4, Annapolis, Maryland, USA.

Forkert, G., Kager, H., Ries, C, 1997: Rectification of Airborne Scanner Images Using Spline Functions for Modelling Flight Path and Attitude Parameters. Proceedings of the 3rd Joint European Conference & Exhibition on Geographical Information. Vienna, Austria, 1997, pp. 106-115.

Fuchs, C., 1998: Extraktion polymorpher Bildstrukturen und ihre topologische und geometrische Gruppierung. PhD Thesis, Institute of Photogrammetry, Bonn University, DGK-C 502.

Gaisky, D., 2000. Geomorphologic improvement of DTMs especially as derived from laser scanner data. International Archives of Photogrammetry and Remote Sensing, Vol. XXXII/6W8, Ljubljana, Slovenia, pages 70-75.

Haala, N., Brenner, C., and Anders, K.-H., 1998: Urban GIS from Laser Altimeter and 2D Map Data. IAPRS 32 (3/1), pp. 339-346.

Kager, H., Kraus, K., 2001: Height discrepancies between overlapping laser scanner strips: simultaneous fitting of aerial laser scanner strips. Grün, A., Kahmen, H. (eds), Optical 3-D Measurement Techniques V. Department of Applied and Engineering Geodesy, Institute of Geodesy and Geophysics, Vienna University of Technology, pp. 103-110.

Kalliany, R., Leberl, F. (eds.), 2002: Photogrammetric Computer Vision. Proceedings of the ISPRS Commission III Symposium in Graz, Austria, September 9-13, 2002, IAPRS XXXIV-3A.

Kraus, K., with contributions by Jansa, J. and Kager, H., 1997: Photogrammetry Volume 2. Advanced Techniques and Applications. 4th ed., Dümmler Verlag, Bonn.

Kraus, K., 2000: Photogrammetrie Band 3. Topographische Informationssysteme. 1st ed., Dümmler Verlag, Köln.

Kraus, K., Pfeifer, N., 1998: Determination of terrain models in wooded areas with aerial laser scanner data. ISPRS Journal of Photogrammetry and Remote Sensing 53 (4), pp. 193-203.

Kraus, K., Pfeifer, N., 2001. Advanced DTM generation from LIDAR data. International Archives of Photogrammetry and Remote Sensing, Volume XXXIV-3/W4, Annapolis, Maryland, USA.

Lohmann, P., Koch, A., Schaeffer, M., 2000. Approaches to the filtering of laser scanner data. International Archives of Photogrammetry and Remote Sensing, Vol XXXIII, Amsterdam, Netherlands.

Moons, T., Frere, D., Vandekerckhove, J., Van Gool, L., 1998: Automatic modeling and 3D reconstruction of urban house roofs from high resolution aerial imagery. ECCV'98, Lecture notes in computer vision 1406(I), pp. 410-425.

ORIENT, 2000: ORIENT. A Universal Photogrammetric Adjustment System. Product information, examples for applications, further references, URL: http://www.ipf.tuwien.ac.at/produktinfo/orient/html_hjk/orient_e.html

Pfeifer, N., Stadler, P., Briese, Ch., 2001: Derivation of digital terrain models in the SCOP++ environment. Proc. of OEEPE Workshop on Airborne Laserscanning and Interferometric SAR for Detailed Digital Terrain Models, Stockholm, Sweden.

Ries, C., Kager, H., Stadler, P., Ressl, C, 2000: Rektifizierung von Flugzeugscanneraufnahmen mit Hilfe von Spline-Funktionen. In: Seyfert, E. (ed.), Proceedings of the 21st scientific-technical annual conference of the German Association for Photogrammetry and Remote Sensing (DGPF), Konstanz, Germany, Publications of the German Association for Photogrammetry and Remote Sensing Vol. 10, September 2001, pp. 229-236.

Ries, C., Kager, H., Stadler, P., 2002: GPS/IMU-unterstützte Georeferenzierung der Daten flugzeuggetragener multispektraler Scanner. In: Proceedings of the 22nd scientific-technical annual conference of the German Association for Photogrammetry and Remote Sensing (DGPF), Neubrandenburg, Germany, 2002 (in print).

Rieger, W., 1992. Automated river line and catchment area extraction from dem data. International Archives of Photogrammetry and Remote Sensing, Vol. XXIX/B4, Washington, USA, pages 642-649.

Rieger, W., Kerschner, M., Reiter, T., Rottensteiner, F., 1999. Roads and buildings from laser scanner data within a forest enterprise. International Archives of Photogrammetry and Remote Sensing, Vol. XXIX/B4, pages 642-649, Washington, DC, USA.

Schenk, T., 2001: Modeling and Recovering Systematic Errors in Airborne Laser Scanners. Torlegård, K. (ed.), Proceedings of OEEPE workshop on Airborne Laserscanning and Interferometric SAR for Detailed Digital Elevation Models, 1-3 March 2001, Royal Institute of Technology, Department of Geodesy and Photogrammetry, Stockholm, Sweden.

Sithole, G., 2001. Filtering of laser altimetry data using a slope adaptive filter International Archives of Photogrammetry and Remote Sensing, Volume XXXIV-3/W4, Annapolis, Maryland, USA.

Von Hansen, W., Vögtle, T., 1999. Extraktion der Geländeoberfläche aus flugzeuggetragenen Laserscanner-Aufnahmen. Photogrammetrie Fernerkundung Geoinformation, 4/1999, pp. 229-236.

Vosselman, G., 2002: On the estimation of planimetric offsets in laser altimetry data. IAPRS 34 (3A), pp. 375-380.

Vosselman, G., Dijkman, S., 2001: 3D building model reconstruction from point clouds and ground plans. IAPRS 34 (3W4), pp. 37-43.

Vosselman, G., Maas, H.-G., 2001: Adjustment and Filtering of Raw Laser Altimetry Data. Torlegård, K. (ed.), Proceedings of OEEPE workshop on Airborne Laserscanning and Interferometric SAR for Detailed Digital Elevation Models, 1-3 March 2001, Royal Institute of Technology, Department of Geodesy and Photogrammetry, Stockholm, Sweden

Vosselmann, G., Maas, H., 2001. Adjustment and Filtering of Raw Laser Altimetry Data. Proceedings of OEEPE Workshop on Airborne Laserscanning and Interferometric SAR for Detailed Digital Terrain Models, Stockholm, Sweden.

Weidner, U., 1997: Gebäudeerfassung aus digitalen Oberflächenmodellen. PhD Thesis, Institute of Photogrammetry, Bonn University, DGK-C 474.

Ziegler, M., Wimmer, A., Wack, R., 2001. DTM generation by means of airborne laser scanning – an advanced method for forested areas. Proceedings of 5th Conference on Optical 3-D measurement techniques, Vienna, Austria.

ACKNOWLEDGEMENTS

This research has been supported by the Austrian Science Foundation (FWF), projects no. P14083 and P15789.